nature communications

Article

https://doi.org/10.1038/s41467-025-59360-7

Electrostatically mediated phosphorescence enhancement of micro-nano composites

Received: 6 November 2024

Accepted: 15 April 2025

Published online: 06 May 2025

Check for updates

Wensheng Xu[1], Guoyi Bai[2], Tingting Li[1], Li Gao[1], Xilong Yan[1,3,4,5], Yang Li[1,4], Ligong Chen[1,3,4,5] ✉ & Bowei Wang[1,3,4,5] ✉

Organic room-temperature phosphorescent materials have developed rapidly. However, the phosphor emission enhancement of micro-nano materials achieved by electrostatic interaction were rarely reported. Herein, taking polystyrene microspheres (μPS) and urea-formaldehyde phosphorescent resin microspheres (μUF) as examples, a method was developed to enhance the phosphorescent performance of μUF by mixing with μPS. The opposite surface potential of μPS and μUF resulting in a significant electrostatic interaction. Moreover, the guest molecules in μUF were polarized under electrostatic interaction, which enhanced the binding to the matrix and further suppressed the non-radiative transition, so effectively improving phosphor emission. Furthermore, the electrostatic interaction of micro-nano composites demonstrated good universality in improving phosphorescence performance, as evidenced by incorporating of varying polymer microparticles into μUF or blending μPS with other phosphorescent microspheres. This work demonstrates the mechanism of electrostatic interaction enhancing phosphorescence emission within the micro-nano composites, which paves the way for the regulation of phosphorescent materials.

Room temperature phosphorescent materials (RTP) have the characteristics of long lifetime phosphorescence[1,2] and large Stokes shift[3,4], which makes them widely used in lighting, display[5], chemical sensing[6,7], biological imaging[8–10] and anti-counterfeiting encryption[11–13]. Traditional long afterglow phosphorescent materials were usually designed and developed based on transition metal ions or rare earth ions[14–17], which required processing of mineral resources, leading to irreversible environmental damage. While, pure organic room temperature phosphorescent (PRTP) materials[18] have become competitive new-type phosphorescent materials because of wide source of raw materials, low toxicity, and good processability. In order to further improve the phosphorescence emission efficiency of PRTP materials, based on the phosphorescence generation mechanism[19], recent reports mainly focused on improving the inter-system crossing (ISC) rate and inhibiting the nonradiative transition and quenching of triplet excitons[20]. Tang et al.[21] reported a cluster exciton model of phosphorescence, in which 1,8-naphthalic anhydride dissolved in an organic solid matrix achieved ultra-long RTP through electron transfer between the matrix and guest molecules, with a lifetime (τ_p) of 600 ms and a total quantum yield (Φ) of more than 20%. Liu et al.[22] improved the phosphorescence emission efficiency by the inclusion of bromobenzyl pyridine with cucurbit[6]uril, which resulted in a promotion of Φ from 24% to 81%. In addition, methods such as molecular engineering[23,24], crystal engineering[25,26], polymer doping[27–29], and carbon dots[30,31] were also efficient ways to construct PRTP materials. However, the dynamically tunable phosphorescent materials were still rarely reported. In addition to the response to quenching factors, such as oxygen[32,33] and water[34,35], other phosphorescent response properties of materials have not been studied in depth. This may be due not only to the lack of theoretical guidance on the regulation of

[1]School of Chemical Engineering and Technology, Tianjin University, Tianjin 300350, P.R. China. [2]School of Chemistry and Chemical Engineering, Tianjin University of Technology, Tianjin 300382, P.R. China. [3]Zhejiang Institute of Tianjin University, Shaoxing 312300, P.R. China. [4]Collaborative Innovation Center of Chemical Science and Engineering (Tianjin), Tianjin 300072, P.R. China. [5]Tianjin Engineering Research Center of Functional Fine Chemicals, Tianjin 300350, P.R. China. ✉e-mail: lgchen@tju.edu.cn; bwwang@tju.edu.cn

phosphorescence properties, but also to the lack of material processing methods to achieve dynamic response in PRTP materials. Therefore, by exploring the dynamic response behavior of phosphorescent materials, the application range and effect of phosphorescent materials would be significantly improved.

Micro-nano materials also show broad application prospects in the field of PRTP because of their unique characteristics[2,36–38] such as micro-scale, low density, large specific surface area and high surface energy. Song et al.[39] prepared phosphorescent carbon dots based on the crosslinking of phthalic anhydride and ethylenediamine, which exhibited an extremely long τ_p ranging from 193 ms to 1.13 s. Xu et al.[40] reported the self-assembly of polyethylene oxide into nanoparticles with enhanced RTP properties, of which the phosphorescence intensity varied with nanoparticles morphology: micelle <nanowire <vesicle. However, in addition to the influence of the size of micro-nano particles on their photophysical properties, the electrostatic interaction also shows potential value in mediating their photophysical properties. Driven by van der Waals force or electrostatic force, micro-nano materials are usually prone to agglomerate randomly in three-dimensional directions[41,42]. The agglomerates in stable state have higher dispersion energy barrier. Accordingly, it is expected to achieve the regulation of the photophysical properties of RTP materials.

According to the principle of electrostatic generation, the redistribution of electrons would occur during the process of contact, friction, and separation between the two substances. Highly dielectric constant polymers tend to be positively charged while polymers with low dielectric constant tend to be negatively charged. Herein, based on the electrostatic interaction within the composites, we developed a method to achieve dynamic phosphorescence emission by mixing phosphorescent microspheres with low dielectric constant polymers microspheres. The intrinsic photophysical mechanism of phosphorescence mediated by electrostatic interaction of micro-nano materials was explored. Firstly, 1, 4-diaminobenzene (14DAP) was selected as phosphorescent guest molecule, which was polycondensed with urea and formaldehyde to prepare urea-formaldehyde phosphorescent microspheres (μUF). Then, polystyrene microspheres (μPS) with a lower dielectric constant and μUF were selected as the samples to study the electrostatic interaction on the photophysical performance of the composites. Interestingly, μPS and μUF exhibited opposite potentials with a potential difference of up to 42 mV, which could produce significant electrostatic interactions between them (Fig. 1a). The composites of μPS and μUF exhibited significantly enhanced phosphorescence characteristics with a varying τ_p from 41 ms to 156 ms. Furthermore, the electrostatic interaction of μPS and μUF in the composite was also observed by FTIR and ^{13}C-SSNMR. Meanwhile, experiment and quantum chemical calculation[43] results showed that the electrostatic interaction can effectively polarize the guest molecules, thereby reducing the energy level difference (ΔE_{ST}), increasing the spin-orbit coupling coefficient (SOC). In addition, the enhanced polarity of the phosphorescent guest molecules can further enhance its binding to urea-formaldehyde resin matrix, thus inhibiting the non-radiative transition and promoting the phosphorescence emission. As expected, incorporating varying polymer microparticles into μUF or blending μPS with other phosphorescent microspheres resulted in significant phosphorescence enhancement, indicating that enhanced phosphorescence emission has good universality in micro-nano composites. Therefore, electrostatic interaction between micro-nano materials enriches the enhancement of phosphorescence performance pathways, helps to regulate the photophysical properties of phosphorescent materials, and also provides a new perspective for studying the response mechanism of photophysical processes.

Results

Phosphorescence enhancement of μPS and μUF composites

Two types of smooth surface polymer microspheres, μPS and μUF, were prepared by dispersion polymerization, (Supplementary Fig. 1). The average molecular weight and particle size of μPS were 7023 g/mol and 358.83 nm, while those of μUF were 92303 g/mol and 2.28 μm (Supplementary Fig. 2,3). Furthermore, μUF exhibited fluorescence emission at 361 nm while its delayed luminescence spectrum showed the phosphorescence emission at 432 nm with a significant Stokes shift (Fig. 2a). And the phosphor lifetime decay curve of μUF indicated its τ_p of 41 ms (Fig. 2b). The observed blue afterglow of μUF was consistent with its phosphorescence spectrum (Fig. 2a). Of course, no phosphorescence emission of μPS was observed (Supplementary Fig. 4a). For the composites of μPS and μUF (Supplementary Movie 1 and 2), the phosphor intensity varied as the mass ratio of μPS to μUF increased, and reached the maximum at the mass ratio of 2:1 (Fig. 2d, e and Supplementary Fig. 5). Meanwhile, the τ_p of μPS and μUF composites also varied from 41 ms to 156 ms (Fig. 2c). Therefore, the μUF exhibited interesting enhanced phosphorescence emission after being mixed with μPS.

Electrical properties and molecular structure characterization

The dielectric property of the material is a crucial factor influencing the electrostatic interaction of the microspheres. Specifically, the dielectric constant of μPS and μUF were 6.0 and 8.5, respectively (supplementary Fig. 6). Compared to bulk polystyrene (dielectric constant=2.5) or urea-formaldehyde resins (dielectric constant=6.0), the dielectric constant of μPS and μUF microspheres are significantly increased, indicating that the polymer microspheres have better dielectric properties and stronger ability to store electrostatic charges. Moreover, the polarity of polystyrene and urea-formaldehyde fragments was investigated by electrostatic potential (ESP) analysis. And the molecular polarity index (MPI)[44] was introduced for assessment of polarity of μUF and μPS (supplementary Fig. 7). MPI of UF was 22.04, while that of PS was 6.8. The MPI difference between PS and UF reached 15.24, which showed significant polarity differences. This was consistent with the dielectric constant of μPS and μUF.

Furthermore, the electrical properties of μPS and μUF were characterized in order to investigate the action of electrostatic interaction on their molecular configuration. The surface potential distribution of μPS and μUF were observed by Kelvin probe force microscopy (KPFM) (Supplementary Fig. 8). Interestingly, the surface potential of μPS was positive (Fig. 3a), while that of μUF was negative (Fig. 3d), which facilitated the formation of clusters for μUF and μPS (Fig. 3h). Through sectional analysis of KPFM, the surface potential of μPS and μUF particles could reach 26 mV and −16 mV, respectively (Fig. 3c, f). The opposite potential was conducive to the formation of the electrostatic interaction between μUF and μPS. Furthermore, in the IR spectra of μPS and μUF composites (Fig. 3g), the carbonyl group characteristic peak of μUF shifted to a higher wavenumber, from 1643 to 1654 cm^{-1}. The vibration enhancement of the carbonyl group was attributed to the electrostatic interaction between μUF and μPS. Additionally, ^{13}C-SSNMR spectra of the μUF and μPS composites (Fig. 3i) showed that the carbonyl carbon characteristic peak of μUF shifted from 161.2 ppm to 162.1 ppm. Conversely, the characteristic peaks of benzene ring of μPS shifted slightly to high field, from 129.2 ppm to 128.9 ppm. The above results showed that there was a significant electrostatic interaction between μPS and μUF with heterologous potential, which could effectively enhance their molecular polarization (Fig. 3j). It could be inferred that the phosphorescent guest molecules of 14DAP in μUF would also undergo similar polarization under electrostatic interaction, which might be the essence of enhanced phosphorescence emission.

Mechanism of Phosphorescence Enhancement in μPS and μUF Composites

To further reveal the mechanism of promoting phosphorescence emission of μUF and μPS composites by electrostatic interaction, quantum chemical calculations and electrostatic field simulations were

conducted. The measured potential values of 26 mV and -16 mV were assigned to μPS and μUF microspheres respectively in the COMSOL Multiphysics 6.5 software[45]. As the distance between μPS and μUF reduced to 5 nm, the electric field intensity was gradually strengthened with an intensity of 5 × 10^5 V/m (Fig. 4b). Then, the electric field with intensity of 5 × 10^5 V/m was applied to 14DAP from three directions (X, Y, Z) to simulate the electrostatic interaction on the photophysical processes and molecular energy levels. As shown in Fig. 4c, 14DAP showed the characteristics of local excitation (LE). In the electron-hole heat map of 14DAP T1 state (Supplementary Fig. 9, 10), the electrons and holes overlapped completely, and the distance (*D*) between the two centers was 0 Å (Supplementary Table 1). Under the action of external electrostatic field, the electrons and holes in the T1 state of 14DAP still maintained a good overlap, and the electron-hole separation degrees (*t*) were from −0.612 Å to −1.102 Å (Supplementary Table 1). The results demonstrated that the T1 state of 14DAP was dominated by LE. Furthermore, the energy level difference of 14DAP was 1.5 eV without electrostatic field, and $\xi(S_0\text{-}T_1)$ remained at an extremely low level of 0 cm^{-1}. With the electric field applied along the X, Y, or Z directions, $\Delta E_{S1\text{-}T2}$ of 14DAP decreased to 0.125 eV, 0.519 eV, and 0.529 eV, respectively (Supplementary Fig. 11). Specifically, the external electric field along Z axis could effectively increase the $\xi(S_0\text{-}T_1)$ to 0.14 cm^{-1} (Fig. 4c). Considering that 14DAP was doped in μUF through co-polycondensation with urea and formaldehyde, the structural fragment of 14DAP urea aldehyde copolymer (14DAP-UF) was calculated under applied electric field (Supplementary Fig. 12). Under the electrostatic field along X-axis, the ΔE_{ST} of 14DAP-UF decreased from 0.536 eV to 0.025 eV, and the $\xi(S_0\text{-}T_1)$ increased from 0.97 cm^{-1} to

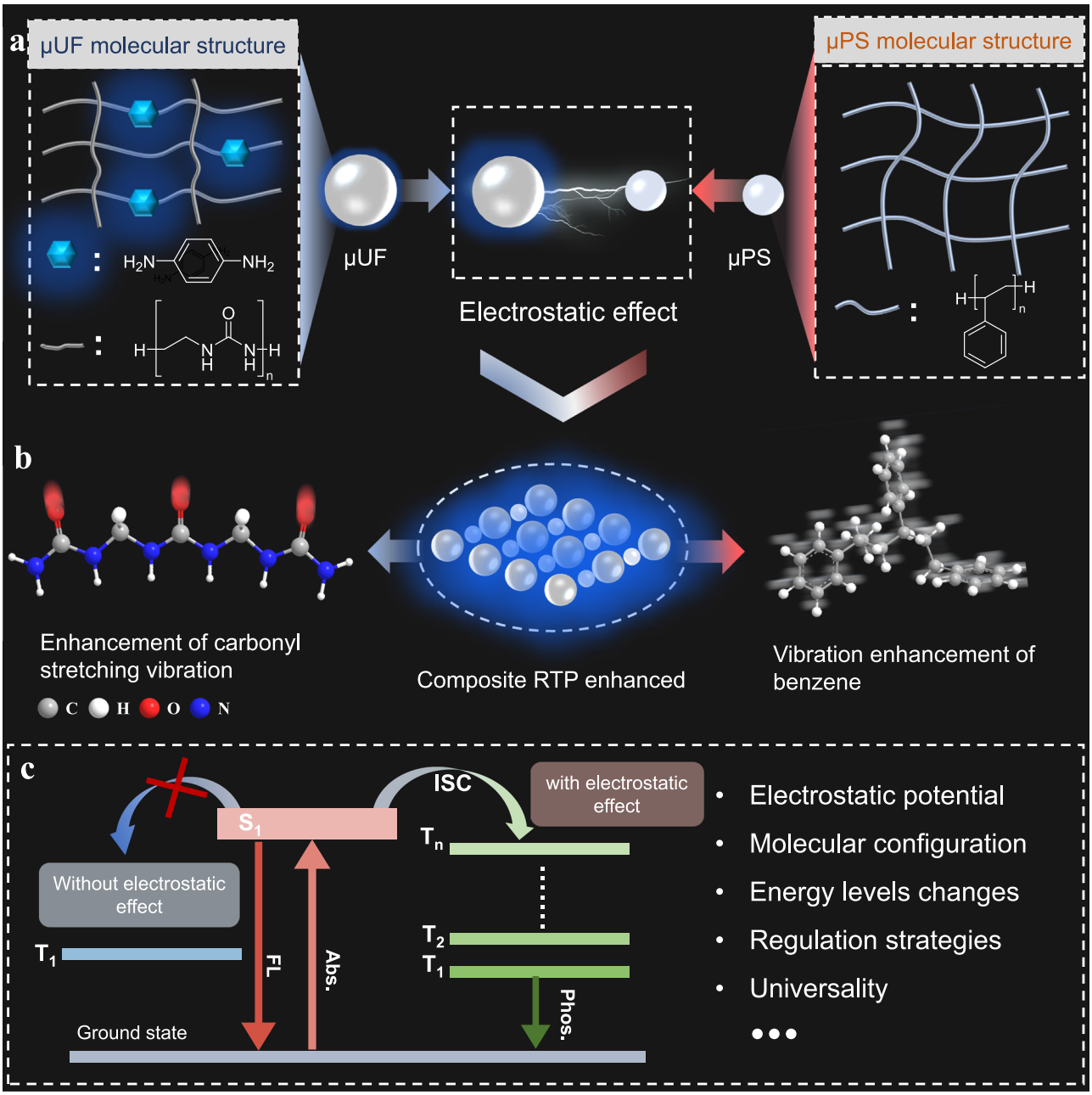

Fig. 1 | Mechanism of phosphorescence emission enhanced by electrostatic interaction. a μUF and μPS molecular structure and electrostatic interaction in the composite; **b** RTP and molecular vibration enhancement within μUF and μPS composites; **c** the mechanism of phosphorescence emission mediated by electrostatic interaction.

https://doi.org/10.1038/s41467-025-59360-7

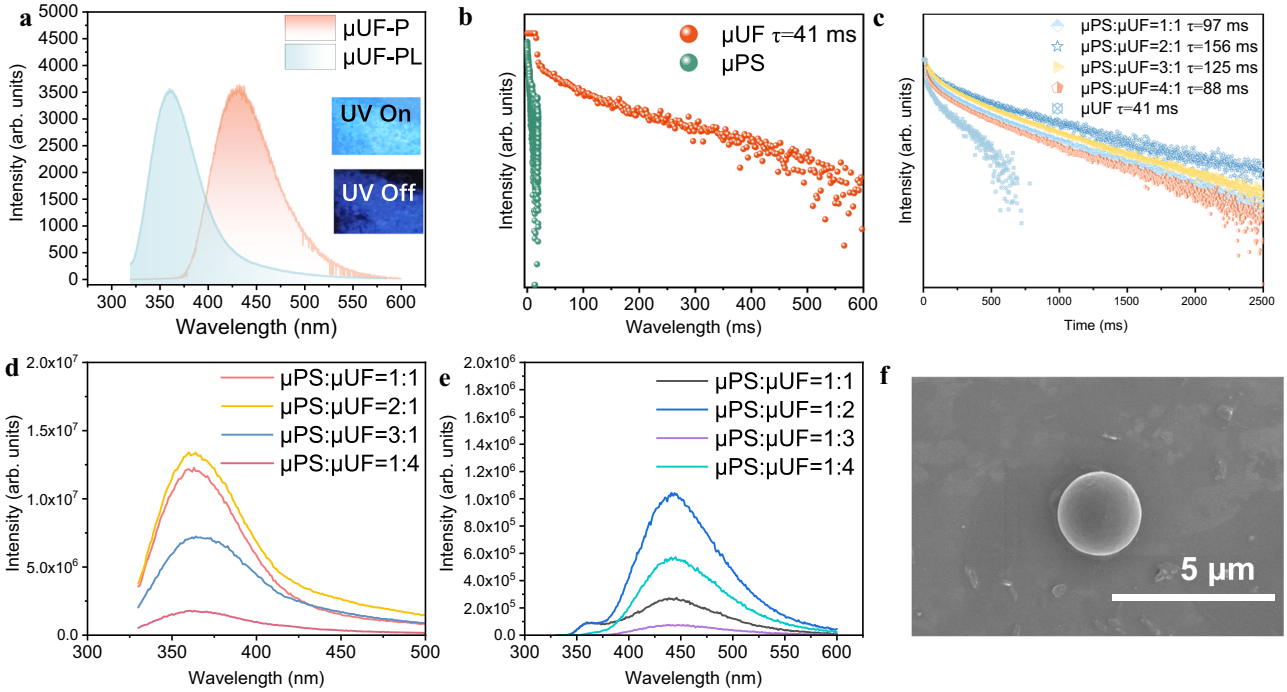

Fig. 2 | Photophysical properties of micro-nano composites. a μUF photoluminescence spectrum, delayed luminescence spectrum (delay time=1 ms) and photoluminescence photos; **b** the phosphor decay lifetime curves of μUF and μPS; **c** phosphor decay lifetime curves and fitting phosphor decay lifetime of composites of μPS and μUF; **d** photoluminescence spectra and **e** phosphorescence spectra of the composites of μPS and μUF. **f** SEM image of μUF. Source data are provided as a Source Data file.

1.84 cm^{-1} (Supplementary Fig. 13b). Therefore, the electrostatic interaction of micro-nano composite materials could promote the phosphorescence emission efficiency by reducing ΔE_{ST} and increasing SOC.

Based on the above work, we further measured the phosphor emission rate (k_p) and the intersystem crossing rate (k_{ISC}) to more accurately demonstrate the effect of electrostatic interaction on the photophysical properties of μUF. As shown in Table 1, τ_f of μUF was 6.40 ns, and the τ_f of the composites showed a trend of decreasing first and then increasing after mixing with μPS. When μUF: μPS is 1:2, the τ_f decreased to the minimum of 6.10 ns, and the k_{ISC} of μUF increased from 14.89×10^7 s^{-1} to 15.58×10^7 s^{-1}. In addition, the k_p of μUF was also greatly improved from 0.040941 s^{-1} to 0.572892 s^{-1}. The results demonstrated that μUF composited with μPS could improve k_{ISC} and k_p, and promoted the phosphorescence emission. It was worth noting that in the quantum chemistry calculation, we found that the $\xi_{(S0\text{-}T1)}$ of the phosphorescent guest molecule was also significantly improved from 0.97 cm^{-1} to 1.84 cm^{-1} under an applied electric field (Supplementary Fig. 13), indicating that the triplet exciton of phosphorescent guest molecule was more likely to return to the ground state by phosphorescent emission. The theoretical calculation results are in good agreement with our experimental results.

To examine whether there existed energy transfer between μPS and μUF microspheres, the UV absorption spectra of μPS and μUF were collected. The results showed that the UV absorption of μUF ranged from 200 to 280 nm, while the photoluminescence spectrum of μPS peaked at 310 nm (Supplementary Fig. 14a). There was no significant overlap between photoluminescence spectrum of μPS and the UV absorption spectrum of μUF. Furthermore, the photoluminescence spectra of μPS and μUF composites were supplemented, and it was found that when the mass ratio of μUF in the composite increased from 0.01 to 0.5, the fluorescence peak intensity at 360 nm continued to increase, while the emission peak of μPS at 310 nm did not show a significant decrease (Supplementary Fig. 14b). In addition, with the increase of mass ratio of μUF, the fluorescence decay spectra of the composites were consistent with that of μPS, and there was no obvious attenuation (Supplementary Fig. 14c). It can be concluded that there is no obvious energy transfer between μPS and μUF. Moreover, we further evaluated the energy transfer process between 14DAP and urea-formaldehyde resin by the UV absorption spectra and photoluminescence spectra. The results showed that the photoluminescence spectra of UF overlaps significantly with the UV absorption of 14DAP at 320 nm–350 nm, which indicated the possibility of energy transfer (Supplementary Fig. 14d). Further, 14DAP was doped into UF at 0.1 wt%, 0.5 wt%, 1 wt%, 5 wt% and 10 wt% respectively, and the UF fluorescence attenuation process was observed (Supplementary Fig. 14e). It could be found that the fluorescence emission of UF at 330 nm was attenuated when 0.1 wt% of 14DAP was doped. When doped with 5 wt% of 14DAP, UF fluorescence emission at 330 nm was completely quenched, indicating that there was an energy transfer process between UF and 14DAP.

In addition, the electrostatic interaction between μUF and μPS in the composites promoted the polarization of the phosphorescent guest molecule 14DAP in μUF (Supplementary Data 1 and 2). Under the electric field, ESP distribution range of 14DAP expanded from −33.6–30.2 kcal/mol to −39.2–56.0 kcal/mol, and the MPI index of 14DAP increased from 13.56 to 15.99 (Supplementary Fig. 15). The polarity of 14DAP was effectively enhanced under electrostatic interaction. Furthermore, the binding energy of 14DAP and urea-formaldehyde resin varied from −24.62 to −27.22 kcal/mol under an electric field (Supplementary Fig. 16). The results indicated that electrostatic interaction enhanced the binding force between the matrix and phosphorescent guest molecules.

In summary, the electrostatic interaction between μPS and μUF in the composites can effectively promote the polarization of 14DAP, enhance its binding with the matrix and inhibit non-radiative transitions. Moreover, the electrostatic interaction reduced ΔE_{ST} and increased SOC of the guest molecules to improve k_{ISC} and k_p, which facilitated the phosphorescent emission efficiency.

https://doi.org/10.1038/s41467-025-59360-7

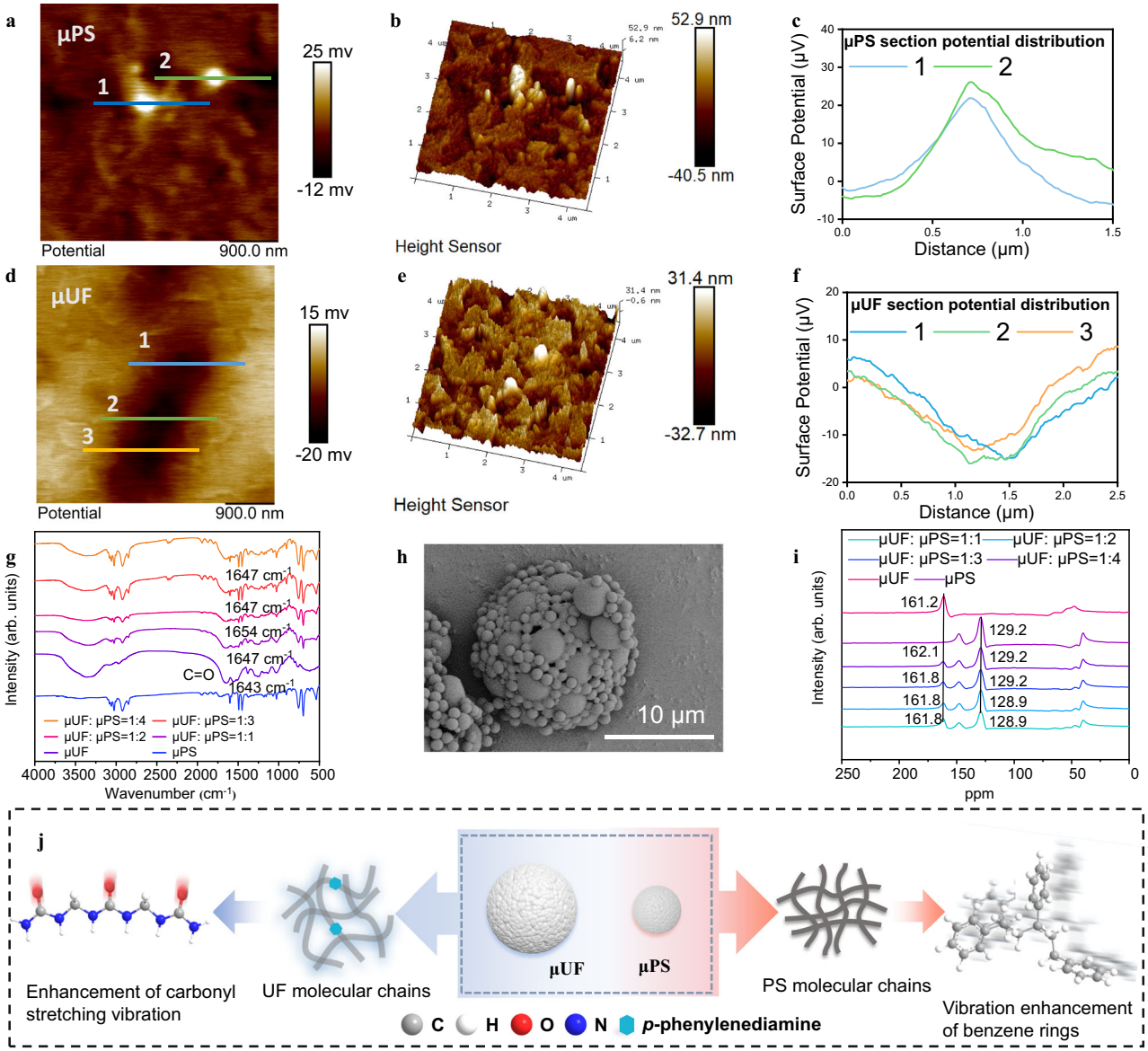

Fig. 3 | Electrostatic interaction on the composites of μPS and μUF. a Potential distribution, **b** height distribution and **c** section potential distribution of μPS in Fig. 3a; **d** potential distribution, **e** height distribution and **f** section potential distribution of μUF in Fig. 3d; **g** IR spectra of μUF and μPS composite; **h** SEM image of μPS and μUF composite; **i** ^{13}C-SSNMR of the composites of μUF and μPS; **j** schematic diagram of molecular configuration changes of μPS and μUF under electrostatic interaction. Source data are provided as a Source Data file.

Effect of polarity difference between two kinds of microspheres on phosphorescence properties of micro-nano composites

According to the triboelectric series of polymers, a more polar material has a higher dielectric constant and tends to acquire a positive charge upon contact with a less polar material. The greater the difference between the dielectric constants of the two materials, the more electrostatic charge would be generated after friction, resulting in a larger surface electrostatic potential. Based on the above work, polymer microspheres with different polarities may exhibit different electrostatic interactions when mixed with μUF, which subsequently influence the phosphorescence properties of μUF. Herein, copolymer microspheres of PS-GMA were synthesized from styrene (St) and glycidyl methacrylate (GMA). Then, PS-GMA was modified using 5-aminotetrazole (5 N) to yield a series of PS-GMA-5N microspheres (Fig. 5b, c) exhibiting varying polarity, including PS-GMA-0.2, PS-GMA-0.5, PS-GMA-0.7, PS-GMA-1.0 (Supplementary Fig. 17). Based on the ESP analysis, MPI of St-GMA modified with 5-aminotetrazole (5 N) increased from 9.76 to 15.05 (Fig. 5a), suggesting that 5 N could effectively enhance the polarity of the microspheres. Furthermore, in the dielectric constant test of PS-GMA-5N microspheres (Supplementary Fig. 18a), it was found that with the increase of the amount of 5 N, the dielectric constant of the microsphere increased from 4.5 to 11, indicating that the polarity of the microsphere was significantly improved. The continuous enhancement of the amino characteristic peak at 3400 cm^{-1} in the IR spectra serves as evidence for the successful preparation of the PS-GMA-5N microspheres (Fig. 5d). Furthermore, X-ray photoelectron spectroscopy (XPS) analysis revealed that PS-GMA-1.0 displayed the highest N content of 3.38% (Supplementary Fig. 18b). Electrochemical impedance spectroscopy (EIS) analysis (Fig. 5e) revealed that the electrochemical impedance of PS-GMA-5N decreased as the content of 5 N increased (ranging from PS-GMA-0.2 to PS-GMA-1.0). Notably, PS-GMA-1.0 exhibited the lowest electrochemical impedance, approaching the value of μUF. The above results showed that the polarity difference with μUF was continuously

https://doi.org/10.1038/s41467-025-59360-7

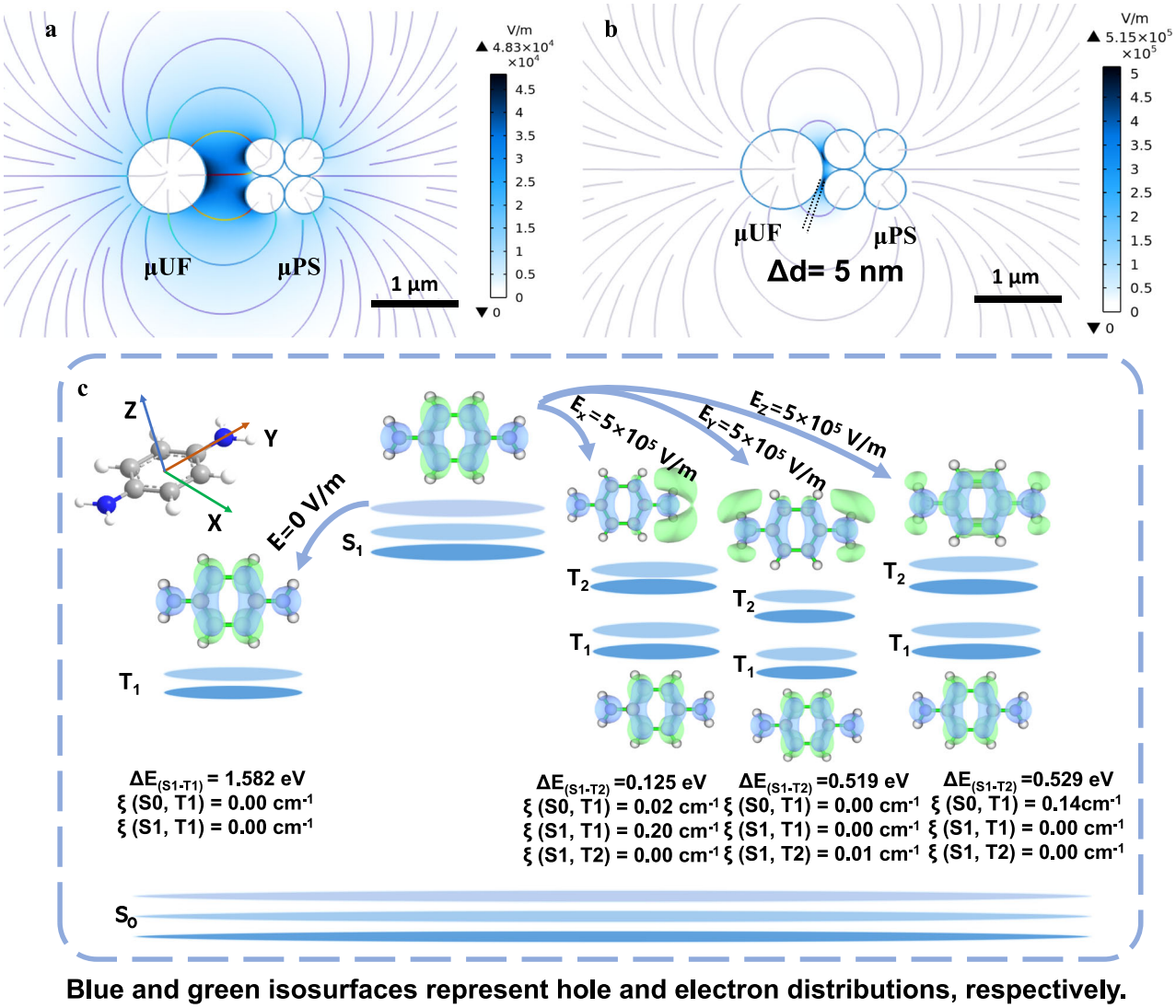

Fig. 4 | Simulation and quantum chemical calculation. Finite element simulation of electrostatic interaction of μUF and μPS during **a** separation and **b** contact. **c** Electron-hole distribution, energy level and SOC of 14DAP under electrostatic fields along X, Y, and Z. Source data are provided as a Source Data file.

Table. 1 | photophysical properties of μUF and μPS composites at room temperature

Sample	λ_{em} (nm)	τ_f (ns)	τ_p (s)	Φ_f (%)	Φ_p (%)	Φ_{isc} (%)	k_f ($10^6 s^{-1}$)	k_p (s^{-1})	k_{isc} ($10^7 s^{-1}$)	$k_{p,\ nr}$ (s^{-1})
μUF	432	6.4	0.8	1.526	3.123	95.351	0.238438	0.040941	14.89859	1.2090592
μUF:μPS = 1:1	432	6.21	0.097	1.947	5.162	92.891	0.313527	0.572892	14.95829	9.7363865
μUF:μPS = 1:2	432	6.1	0.156	2.051	2.901	95.048	0.33623	0.19565	15.58164	6.2146063
μUF:μPS = 1:3	432	7.54	0.125	1.151	2.106	96.743	0.152653	0.174152	12.83064	7.8258479
μUF:μPS = 1:4	432	7.59	0.88	1.437	2.628	95.935	0.189328	0.031129	12.63966	1.1052346

Where λ_{em} refers to emission wavelength; τ_f and τ_p refer to the lifetime of fluorescence and phosphorescence; Φ_f, Φ_p and Φ_{isc} refer to the quantum yield of fluorescence (Supplementary Fig. 4c-g), phosphorescence and intersystem crossing; k_f and k_p refer to radiative decay rate of fluorescence and phosphorescence; k_{isc} refers to intersystem crossing rate; k_p, nr refers to nonradiative decay rate of phosphorescence.

decreasing from PS-GMA-0.2 to PS-GMA-1.0. Finally, micro-nano composites were obtained by mixing PS-GMA-5N and μUF, in which the τ_p of PS-GMA-0.2 and μUF composite was 151 ms (Fig. 5f, g). From PS-GMA-0.2 to PS-GMA-1.0, the phosphorescence performance of the μUF composites decreased continually (Fig. 5f), and the τ_p of PS-GMA-1.0 and μUF composite was 91 ms (Fig. 5g). Therefore, as the polarity difference between PS-GMA-5N and μUF decreases, the electrostatic interaction of them was also weakened, resulting in decrease in τ_p of their composites.

Universality of electrostatically mediated phosphorescence enhancement of micro-nano materials

To further explore the universality of electrostatically mediated phosphorescence enhancement of micro-nano materials. Various composites were prepared by mixing μUF with kinds of polymer microspheres, including polyethylene (PE), polyvinyl chloride (PVC), polymethyl methacrylate (PMMA), polyamide (PA), and polyacrylonitrile (PAN). Subsequently, the phosphorescence properties of these composites were evaluated. Among them, at a mass ratio of μUF

https://doi.org/10.1038/s41467-025-59360-7

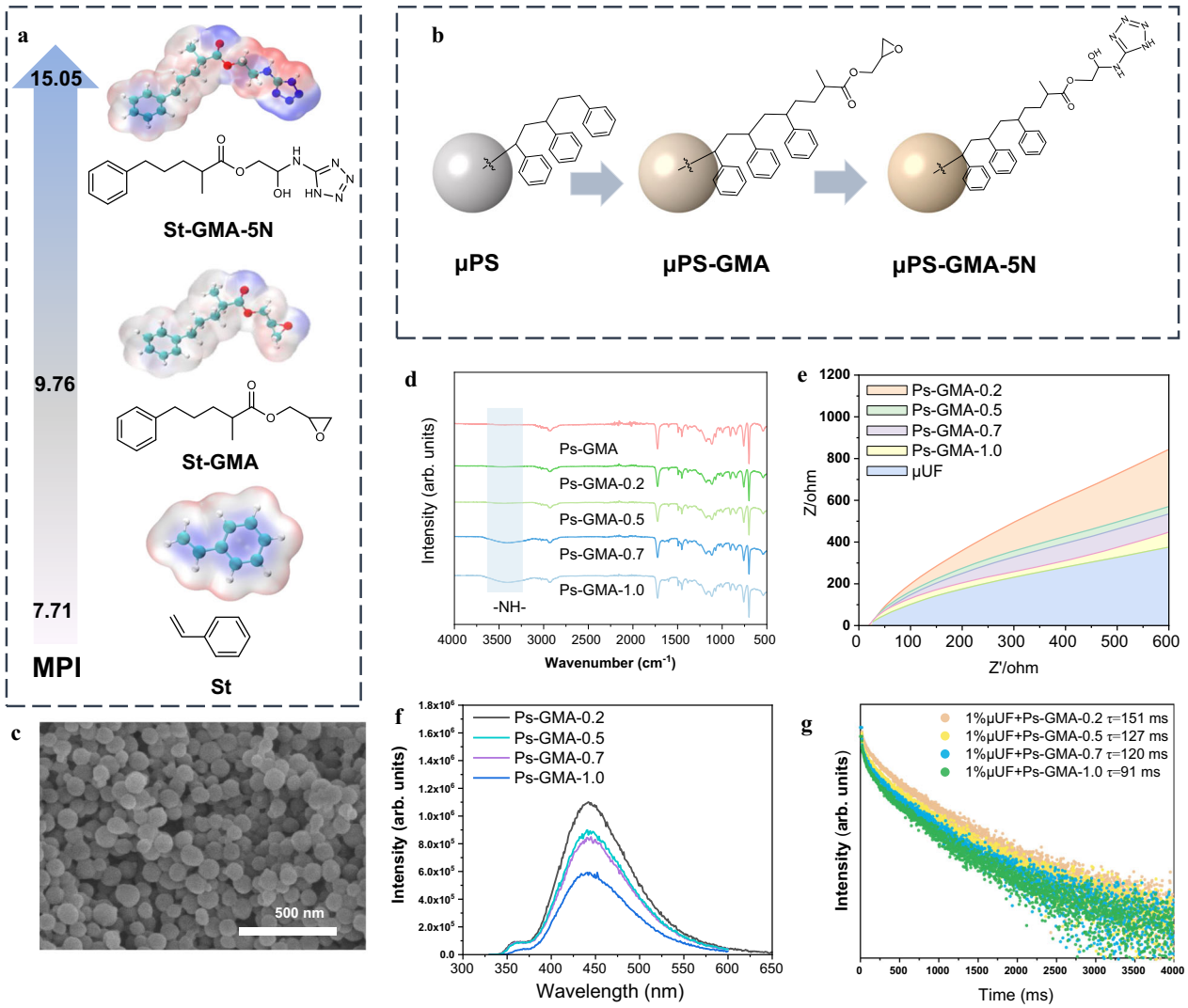

Fig. 5 | Effect of polarity difference between polymer microspheres and μUF on the phosphorescence performance of micro-nano composites. a ESP and MPI calculation of St, St-GMA, and St-GMA-5N; **b** modification of μPS with 5 N. **c** SEM image of μPS-GMA. **d** IR spectra of PS-GMA and PS-GMA-5N; **e** EIS of μPS-GMA-5N and μUF; **f** delayed luminescence spectra and **g** phosphorescence decay lifetime spectra of composites of PS-GMA-5N and μUF. Source data are provided as a Source Data file.

to PA particle of 1:2, the composite demonstrated a τ_p of 89 ms (Supplementary Fig. 19c), whereas the PE and μUF composites exhibited a longer τ_p of 226 ms (Supplementary Fig. 19i). Further, as the mass ratio of PE to μUF increased to 1:1, the τ_p of the composites could reached 252 ms (Supplementary Fig. 19i). It was worth mentioning that μUF mixed with other polymer microspheres also showed an improvement of τ_p. Thus, the phosphorescence emission of μUF can be effectively enhanced by the electrostatic interaction between polymer and μUF microspheres of the obtained composites by mixing μUF with various polymer microspheres.

In addition, a series of urea-formaldehyde resin phosphor microspheres were prepared by selecting a series of phosphor guest molecules, and the phosphor properties of the urea-formaldehyde resin phosphor microspheres and μPS composites were evaluated. Considering that amino or aldehyde groups contained in phosphorescent guest molecules can be involved in the polycondensation reaction to form urea-formaldehyde resin copolymers, a variety of aromatic compounds containing amino, formyl or non-functional groups were selected as phosphorescent guest molecules (Supplementary Movie 3–7), including 3,4-dimethoxybenzaldehyde (DMBD), 2,3-diaminonaphthalene (23DAN), 9-aminophenanthrene (9AP), vanillin acetate (VA) and phenanthrene (Phn). Accordingly, the corresponding urea-formaldehyde resin phosphorescent microspheres, such as μDMBD/UF, μ23DAN/UF, μ9AP/UF, μVA/UF and μPhn/UF, were prepared, as shown in Supplementary Fig. 20. As expected, the delayed luminescence spectra of these urea-formaldehyde resin phosphorescent microspheres all exhibited obvious phosphorescence emission (Fig. 6a–e). Subsequently, a series of composites were prepared by blending the urea-formaldehyde resin phosphorescent microspheres with μPS at a mass ratio of 1:2 (Supplementary Fig. 21). The τ_p of the composites exhibited an improvement compared to that of the urea-formaldehyde resin phosphorescent microspheres. (Fig. 6f). Specifically, the τ_p of μDMBD/UF increased from 38 ms to 77 ms after mixing with μPS (Fig. 6f). Similarly, the τ_p of μPhn/UF and μPS composite increased from 565 ms to 903 ms (Fig. 6f). Therefore, for phosphor guest molecules, the phosphorescence emission can also be effectively enhanced by the electrostatic interaction between the urea-formaldehyde resin phosphor microspheres and μPS.

In summary, the phosphorescent enhancement of micro-nano composites could be achieved by mixing μUF with different polymer microspheres or different phosphorescent microspheres with μPS, demonstrating a good universality of electrostatically mediated phosphorescence enhancement of micro-nano composites. This has

https://doi.org/10.1038/s41467-025-59360-7

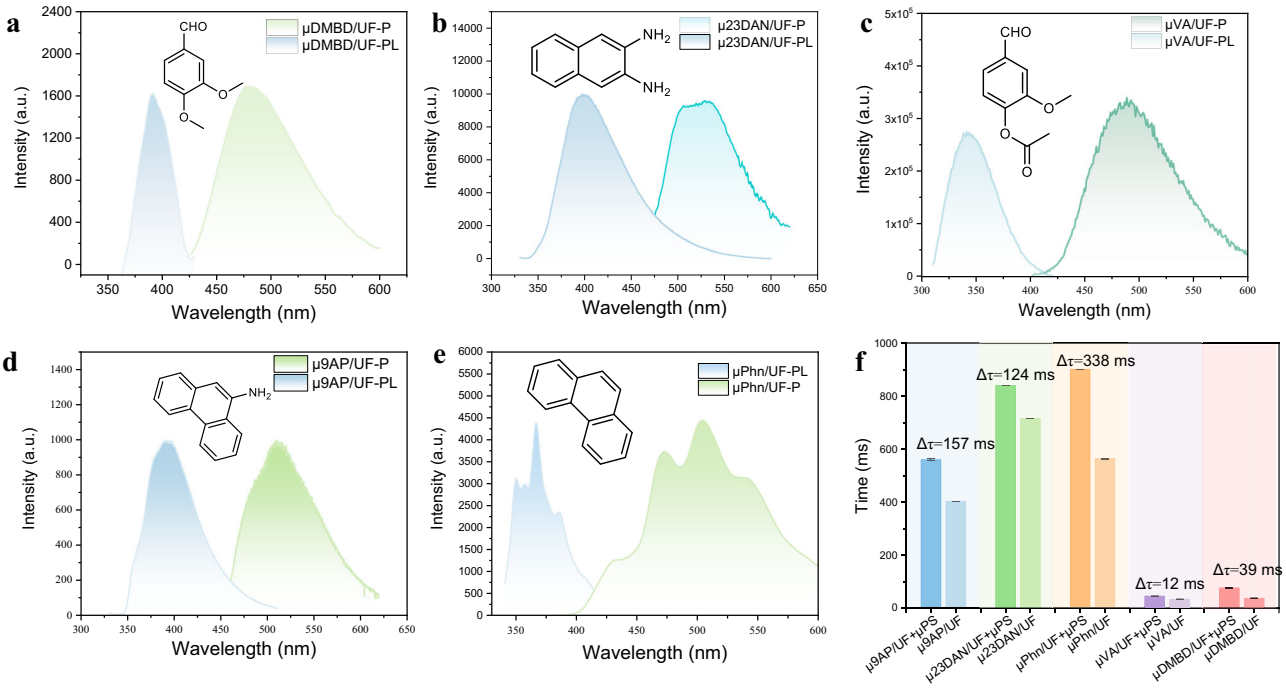

Fig. 6 | Universality of enhanced RTP emission of micro-nano composites. Photoluminescence spectra and delayed luminescence spectra of **a** μDMBD/UF, **b** μ9AP/UF, **c** μ23DAN/UF, **d** μPhn/UF, **e** μVA/UF. **f** The phosphorescence decay lifetime of various phosphorescent microspheres and the composites. The bar chart with error bar is obtained by taking the mean and standard deviation of three times of decay lifetime measured for each sample. Δτ was the lifetime difference before and after mixing the samples with μPS. Source data are provided as a Source Data file.

paved the way for the development of more efficient and tunable phosphorescent materials.

Discussion

In summary, based on the electrostatic interaction of micro-nano composites, the phosphorescence characteristics of urea-formaldehyde resin microspheres were dynamically mediated. Taking the composite of μPS and μUF as an example, the τ_p of the composite was increased from 41 ms to 156 ms and the phosphor intensity was also enhanced. Their KPFM spectra showed that μPS and μUF exhibited opposite surface potentials and could produce obvious electrostatic interaction. Thus, after mixing μUF with μPS, the stretching vibration peak of carbonyl group in μUF shifted to a higher wavenumber in the IR spectra. Meanwhile, the peaks of carbonyl carbon and benzene ring in their ^{13}C solid state NMR spectra shifted to low field and high field, respectively, indicating the electrostatic interaction of the composites. By mixing μUF with a series of PS-GMA-5N polymer microspheres of different polarities, the photophysical properties of composites varied with the polarity. It was found that the greater the polarity difference between the two micro-nano materials, the better the phosphorescence performance of the composites. The finite element simulation revealed that the intensity of electrostatic field between μPS and μUF could reach 5×10^5 V/m. Additionally, the electrostatic interaction facilitated the polarization of phosphorescent guest molecules, enhancing their binding with the matrix, reducing the energy level difference, enhancing SOC, and promoting k_{ISC} and k_P. Moreover, when various polymer microspheres mixed with μUF or a variety of phosphorescent urea formaldehyde resin microspheres mixed with μPS, the τ_p of the resulting composites exhibited different degrees of improvement, demonstrating a good universality of electrostatically mediated phosphorescence enhancement of micro-nano composites. Consequently, the electrostatic interaction within micro-nano phosphorescent composites can effectively achieve RTP enhancement, which would broaden the future application of RTP materials in the field of functional devices.

Methods

Materials and methods

All chemicals were purchased from commercial sources without further purification. Urea, styrene (St) and 37-40% formaldehyde solution were purchased from Tianjin Jiangtian Chemical Technology Co., LTD. 1,4-Diaminobenzene (14DAP) was obtained from Shanghai Macklin Biochemical Technology Co. 3,4-Dimethoxybenzaldehyde (DMBD), glycidyl methacrylate (GMA), polyacrylonitrile (PAN) and 5-aminotetrazole (5 N) were purchased from Tianjin Heowns Biochemical Technology Co., Ltd. 2,3-Diaminonaphthalene (23DAN), 9-aminophenanthrene (9AP) and vanillin acetate (VA) were obtained from Shanghai Bide Pharmatech Co., Ltd. Phenanthrene (Phn) was purchased from Shanghai Dibai Chemical Technology Co., Ltd. polyethylene (PE), polyvinyl chloride (PVC), polymethyl methacrylate (PMMA), and polyamide (PA) microparticles were purchased from Dongguan Zhangmu Suzhan plastic Co., LTD.

Photoluminescence spectra, delayed photoluminescence spectra, and phosphor life decay curves were performed on a F-4700 fluorescence spectrophotometer (HITACHI Instruments, Japan). Infrared spectra (IR) were measured on a Nicolet 380 FT-IR spectrometer (ThermoFisher Scientific, America). X-ray diffraction (XRD) analyses were carried out on AXS D8 X-ray diffractometer (Bruker, America) using a Cu Kα X-ray source (40 kV, 100 mA). X-ray Photoelectron Spectroscopy (XPS) was performed using a Kalpha (ThermoFisher Scientific, America). Kelvin Probe Force Microscope (KPFM) spectra were collected by Bruker Dimension Atomic Force Microscope. Dielectric properties were tested by Agilent 4294 A. Electrochemical properties of materials were measured through a three-electrode system in an electrochemical workstation with a brand of CHI66 (Chenhua, China).

Preparation of samples

μPS. Deionized water (100.0 mL), ethanol (20.0 mL), polyacrylic acid (0.5 g) and potassium persulfate (0.1 g, 0.37 mmol) were added to a round-bottom flask, and stirred at room temperature. Subsequently, styrene (3.0 g, 28.81 mmol) was added dropwise. Under a nitrogen

atmosphere, it was stirred at room temperature for 30 min, then heated to 75 °C and stirred for 8 h to yield the suspension. Then, the suspension was centrifuged at 8000 rpm with the centrifugal force is 7155 g for 8 min to yield a white solid. After washing the white solid with deionized water five times, the resulting white powder was dried for use.

μUF. Urea-formaldehyde resin microspheres were prepared by dispersion polymerization. Urea (1.5 g, 25.00 mmol), 40% formaldehyde solution (4.1 g, 54.67 mmol), 1, 4-diaminobenzene (40.0 mg, 0.37 mmol), and water (50 mL) were added into a one-neck flask. After dissolution, hydroxymethyl cellulose (50.0 mg, 0.68 mmol) and ammonium sulfate (4.0 g, 28.17 mmol) were added as dispersant and precipitant, respectively. The pH of the reaction solution was adjusted to 2, heated to 50 °C for 3 h, cooled to room temperature and aged for 24 h. The precipitate was filtered, washed for 5 times, and dried at 50 °C for 3 h to obtain μUFs.

μDMBD/UF. DMBD doped urea formaldehyde resin phosphorescent material was prepared by dispersion polymerization. Urea (1.5 g, 25.00 mmol), DMBD (30 mg, 0.18 mmol), 40% formaldehyde solution (4.1 g, 54.67 mmol), and water (50 mL) were added into a one-neck flask. then, hydroxymethyl cellulose (50.0 mg, 0.68 mmol) and ammonium sulfate (4.0 g, 28.17 mmol) were added as dispersant and precipitant, respectively. The pH of the reaction solution was adjusted to 2, heated to 50 °C for 3 h, cooled to room temperature and aged for 24 h. The precipitate was filtered, washed for 5 times, and dried at 50 °C for 3 h to obtain μDMBD/UF.

Following the same synthetic procedure, DMBD was replaced with 23DAN (30 mg, 0.19 mmol), VA (30 mg, 0.15 mmol), Phn (30 mg, 0.17 mmol), or 9AP (30 mg, 0.16 mmol), respectively, to prepare the phosphorescent microspheres μ23DAN/UF, μVA/UF, μPhn/UF, and μ9AP/UF.

μPS-GMA. Potassium persulfate (0.2 g, 0.74 mmol), tween 20 (0.5 g, 0.96 mmol) and deionized water (60.0 ml) were added into a 250 ml one-neck flask. Then, GMA (5.0 g, 35.21 mmol) and St (5.0 g, 48.07 mmol) were dropwise added to the flask, then, it was heated to 75 °C for 8 h to form a white emulsion, and then cooled to room temperature. The reaction mixture was demulsified with ethanol, centrifuged to obtain a white solid, washed repeatedly with ethanol for 5 times, and dried under vacuum at 50 °C to obtain a white powder.

μPS-GMA-5N. μPS-GMA (1.5 g), 5 N (80.0 mg, 0.2 equiv. was relative to GMA of μPS-GMA) and deionized water (100.0 mL) were added into a round-bottom flask. Stirred the mixture for 4 h at 80 °C. Then filter the mixture and vacuum dry the filter cake to obtain the white solid powder μPS-GMA-0.2. Similarly, μPS-GMA-0.5, μPS-GMA-0.7, and μPS-GMA-1.0 were prepared.

Quantum chemical calculation

The ESP distribution and MPI of the molecules were calculated based on the optimized configuration of guest molecules using Multifunctional Wavefunction Analyzer (Mutiwfn).

Gaussain 09 was used to optimize the configuration of guest molecules and their derivatives under the b3lyp/6-31 g(d). The external electric field was applied in X direction, for example, the case of EEF = 0.01 a.u. (1a.u.=5.142206 × 10^{11} V/m) corresponds to using the keyword of field = read 0.01, 0, 0 in Gaussian. Similarly, the keywords in the Y or Z direction are field = read 0, 0.01, 0 or field = read 0, 0, 0.01.

The singlet, triplet, binding energy and SOC of guest molecules and matrix were also calculated under b3lyp/def2-tzvp by ORCA 5.0.

Simulation Modeling

COMSOL Multiphysics 6.2 software and finite element analysis method were used for simulation modelling. Experimentally measured values were input into the software for μPS (dielectric constant = 5.5, surface potential = 26 mV) and μUF (dielectric constant = 8.5, surface potential = −16mV).

Data availability

All the other data used in this study are available in the article and its supplementary information files and from the corresponding author upon request. Source data are provided as a Source Data file.

References

1. Li, J., Wu, Y. & Gong, X. Evolution and fabrication of carbon dot-based room temperature phosphorescence materials. *Chem. Sci.* **14**, 3705–3729 (2023).
2. Wu, C., Wang, A. C., Ding, W., Guo, H. & Wang, Z. L. Triboelectric nanogenerator: a foundation of the energy for the new era. *Adv. Energy Mater.* **9**, 1802906 (2019).
3. Zhou, W.-L., Lin, W., Chen, Y. & Liu, Y. Supramolecular assembly confined purely organic room temperature phosphorescence and its biological imaging. *Chem. Sci.* **13**, 7976–7989 (2022).
4. Yin C. et al. A 3D phosphorescent supramolecular organic framework in aqueous solution. *Mater*. 2316008 (2024).
5. Ye, W. et al. Confining isolated chromophores for highly efficient blue phosphorescence. *Nat. Mater.* **20**, 1539–1544 (2021).
6. Wang, Y., Liu, H., Chen, Z. & Pu, S. Aggregation-induced emission enhancement (AIEE)-active tetraphenylethene (TPE)-based chemosensor for CN^-. *Spectroc. Acta Pt. A-Molec. BioMolec. Spectr.* **245**, 118928 (2021).
7. Cheng, Z. et al. Ultralong phosphorescence from organic ionic crystals under ambient conditions. *Angew. Chem. -Int. Ed.* **57**, 678–682 (2018).
8. Xiong, X. et al. Thermally activated delayed fluorescence of fluorescein derivative for time-resolved and confocal fluorescence imaging. *J. Am. Chem. Soc.* **136**, 9590–9597 (2014).
9. Shi, H. et al. A highly efficient red metal-free organic phosphor for time-resolved luminescence imaging and photodynamic therapy. *ACS Appl. Mater. Interfaces* **11**, 18103–18110 (2019).
10. Zhen, X. et al. Ultralong phosphorescence of water-soluble organic nanoparticles for in vivo afterglow imaging. *Adv. Mater.* **29**, 1606665 (2017).
11. An, Z. et al. Stabilizing triplet excited states for ultralong organic phosphorescence. *Nat. Mater.* **14**, 685–690 (2015).
12. Gu, L. et al. Dynamic ultralong organic phosphorescence by photoactivation. *Angew. Chem. -Int. Ed.* **57**, 8425–8431 (2018).
13. Wang, X. et al. Multicolor ultralong organic phosphorescence through alkyl engineering for 4D coding applications. *Chem. Mat.* **31**, 5584–5591 (2019).
14. Yuan, S., Yang, Y., Xu, Z. & Fang, B. Effect of dopants on long after glow properties of Y_2O_2S: Eu phosphor and its long afterglow mechanism [J]. *J. Inorg. Mater.* **19**, 523 (2004).
15. Yan, W.-z, Lin, L., Chen, Y.-h & Yin, M. New red long afterglow aluminate materials doped with mn^{4+}. *Chin. J. Lumin.* **29**, 114 (2008).
16. Ju, Z.-H., Zhang, S.-H., Gao, X.-P., Tang, X.-L. & Liu, W.-S. Reddish orange long afterglow phosphor Ca_2SnO_4: Sm^{3+} prepared by sol-gel method. *J. Alloy. Compd.* **509**, 8082–8087 (2011).
17. Junying, Z. Synthesis and luminescent properties of long afterglow glass. *J. Chin. Rare Earth Soc.* **21**, 151–154 (2003).
18. Yang, X., Waterhouse, G. I., Lu, S. & Yu, J. Recent advances in the design of afterglow materials: mechanisms, structural regulation strategies and applications. *Chem. Soc. Rev.* **52**, 8005–8058 (2023).
19. Zhao, W., He, Z. & Tang, B. Z. Room-temperature phosphorescence from organic aggregates. *Nat. Rev. Mater.* **5**, 869–885 (2020).
20. Qin, W. et al. Simultaneous promotion of efficiency and lifetime of organic phosphorescence for self-referenced temperature sensing. *Chem. Eng. J.* **400**, 125934 (2020).

21. Zhang, X. et al. Ultralong UV/mechano-excited room temperature phosphorescence from purely organic cluster excitons. *Nat. Commun.* **10**, 5161 (2019).
22. Zhou, X. et al. Supramolecular assembly activated single-molecule phosphorescence resonance energy transfer for near-infrared targeted cell imaging. *Nat. Commun.* **15**, 4787 (2024).
23. Liu, Z.-X. et al. Room-temperature phosphorescence with variable lifetime of halogen-comprising coordination polymers. *Inorg. Chem.* **59**, 17870–17874 (2020).
24. Wang, Z. et al. Recent advances in organic room-temperature phosphorescence of heteroatom (B/S/P) containing chromophores. *CCS Chem.* **5**, 292–309 (2023).
25. Yin, Z. et al. Molecular engineering through control of structural deformation for highly efficient ultralong organic phosphorescence. *Angew. Chem. -Int. Ed.* **133**, 2086–2091 (2021).
26. Nidhankar, A. D., Nayak, R. A. & Babu, S. S. Aggregation-induced phosphorescence of an anthraquinone based emitter. *Org. Biomol. Chem.* **19**, 1004–1008 (2021).
27. Shen, Z. et al. Color-tunable, time-dependent, temperature and humidity-responsive afterglow from hyaluronic acid-based films. *Dyes Pigment* **212**, 111113 (2023).
28. Lin, X., Xu, Q. & Ma, X. Emission-tunable room-temperature phosphorescent polymers based on dynamic reversible supramolecule-mediated photocrosslinking. *Adv. Opt. Mater.* **10**, 2101646 (2022).
29. Yan, Z. A., Lin, X., Sun, S., Ma, X. & Tian, H. Activating room-temperature phosphorescence of organic luminophores via external heavy-atom effect and rigidity of ionic polymer matrix. *Angew. Chem. -Int. Ed.* **60**, 19735–19739 (2021).
30. Sun, Y. et al. Ultralong lifetime and efficient room temperature phosphorescent carbon dots through multi-confinement structure design. *Nat. Commun.* **11**, 5591 (2020).
31. Cui, S. et al. Colorful, time-dependent carbon dot-based afterglow with ultralong lifetime. *Chem. Eng. J.* **431**, 133373 (2022).
32. Keruckiene, R., Volyniuk, D., Leitonas, K. & Grazulevicius, J. V. Dual emission fluorescence/room-temperature phosphorescence of phenothiazine and benzotrifluoride derivatives and its application for optical sensing of oxygen. *Sens. Actuator B-Chem.* **321**, 128533 (2020).
33. Zang, L. & Zhao, H. A strategy for monitoring oxygen concentration, oxygen consumption, and generation of singlet oxygen using a phosphorescent photosensitizer. *J. Lumines* **224**, 117282 (2020).
34. Zhang, X. et al. Irreversible humidity-responsive phosphorescence materials from cellulose for advanced anti-counterfeiting and environmental monitoring. *ACS Appl. Mater. Interfaces* **14**, 16582–16591 (2022).
35. Fan, W.-T. et al. Construction and Humidity Response of a Room-Temperature-Phosphorescent Hybrid Xerogel Based on a Multicharge Supramolecular Assembly. *ACS Appl. Mater. Interfaces* **2**, 2000080 (2021).
36. Wang, Y. et al. The development and progression of micro-nano Optics. *Front. Chem.* **10**, 916553 (2022).
37. Zhou, L., Liu, D., Wang, J. & Wang, Z. L. Triboelectric nanogenerators: fundamental physics and potential applications. *Friction* **8**, 481–506 (2020).
38. Zhai, W. et al. Recent progress on wear-resistant materials: designs, properties, and applications. *Adv. Sci.* **8**, 2003739 (2021).
39. Song, S.-Y. et al. Self-exothermic reaction driven large-scale synthesis of phosphorescent carbon nanodots. *Nano Res.* **14**, 2231–2240 (2021).
40. Xu, W., Yin, D., Pan, C., Liu, C. & Hong, C. Fabrication of nanoobjects with morphology-correlated room-temperature phosphorescence and their application in information encryption. *Poly. Chem.* **14**, 318–323 (2023).
41. Ruan, X., Gorman, M. T., Li, S. & Ni, R. Surface-resolved dynamic simulation of charged non-spherical particles. *J. Comput. Phys.* **466**, 111381 (2022).
42. Xu, W. et al. Urea-formaldehyde resin room temperature phosphorescent material with ultra-long afterglow and adjustable phosphorescence performance. *Nat. Commun.* **15**, 4415 (2024).
43. Lu, T. & Chen, F. Multiwfn: A multifunctional wavefunction analyzer. *J. Comput. Chem.* **33**, 580–592 (2012).
44. Liu, Z., Lu, T. & Chen, Q. Intermolecular interaction characteristics of the all-carboatomic ring, cyclo[18]carbon: Focusing on molecular adsorption and stacking. *Carbon* **171**, 514–523 (2021).
45. Matias, A., Shinbrot, T. & Araújo, N. Mechanical equilibrium of aggregates of dielectric spheres. *Phys. Rev. E* **98**, 062903 (2018).

Acknowledgements

Thanks to Dr. Hu Wanting from Tsinghua University for the support in the analysis of compound structures and characterization of material dielectric properties.

Author contributions

Wensheng Xu: Conceptualization, Investigation, Formal analysis, Validation, Writing-Original Draft, Writing-Review & Editing. Guoyi Bai: Conceptualization, Investigation, Writing-Original Draft. Li Gao: Methodology, Formal analysis. Tingting Li: Data Curation, Formal analysis. Xilong Yan: Data Curation. Yang Li: Methodology. Ligong Chen: Supervision, Project administration, Writing-Review & Editing. Bowei Wang: Supervision, Project administration, Writing - Review & Editing.

Competing interests

The authors declare no competing interest.

Additional information

Supplementary information The online version contains supplementary material available at https://doi.org/10.1038/s41467-025-59360-7.

Correspondence and requests for materials should be addressed to Ligong Chen or Bowei Wang.

Peer review information *Nature Communications* thanks the anonymous reviewer(s) for their contribution to the peer review of this work. A peer review file is available.